EFFECT OF ENERGY INPUT ON POROSITY AND MICROHARDNESS IN LASER CLADDING COATING ON FGS600-3A DUCTILE CAST IRON

[1]Adem KARŞI, [2]Meryem ALTAY, [1]Dilara ERGİN, [2]Hakan AYDIN

[1]Coşkunöz R&D Center, Fethiye Organized Industrial Zone, Bursa, Turkey,
akarsi@coskunoz.com.tr, dergin@coskunoz.com.tr

[2]Engineering Faculty, Mechanical Engineering Department, Bursa Uludag University, Gorukle-Bursa, Turkey,
meryemaltay@uludag.edu.tr, hakanay@uludag.edu.tr

Abstract

Laser cladding, which is surface modification technology, is based on melting with a laser beam by spraying powder on the base metal and generated by depositing the layers. In this study, the Metco 42C martensitic stainless steel powder material was cladded on the FGS600-3A ductile cast iron used in sheet metal forming molds. The effect of energy input on porosity and microhardness was investigated. The digital image processing method was used for porosity analysis. The energy input had a significant effect on the pore formation. The lower energy input (1.1 kW laser power, 14 mm/s scanning speed) resulted in lower porosity. The cladding thickness varied depending on the scanning speed parameter due to affecting powder efficiency, high thickness was obtained at 6 mm/s low scanning speed. In the upper layer of the cladding, high hardness values were achieved due to the martensitic phase formation. The bottom layers of cladding had lower hardness values because of the tempering of the hard martensitic phases by subsequent cladding processes. Significant increase in hardness at cladding zone was attributed to carbon transfer from the base metal. This remarkable increase in hardness was much higher at lowest energy input (1.1 kW laser power and 14 mm/s scanning speed). However, it is clear that this will increase the risk of crack formation because of brittleness. On the other hand, at the higher energy input, this significant increase in hardness is at a lower level due to rest-austenite formation and excessive annealing with subsequent cladding processes.

Keywords: Laser cladding; process parameters; porosity; micro-hardness, martensitic stainless steel powder

1.   INTRODUCTION

The laser cladding, that is surface modification technology and a precision repair method, is based on the principle of melting with a laser beam by spraying powder on the base material. It can be produced by depositing the material in the form of layers of multi-track. This advanced method is preferred in the industry with its advantages such as high energy density during deposition, minimum dilution rate, high production rate, shallow heat-affected zone, minimum distortion, fast cooling, good mechanical properties and good surface quality [1]. Laser cladding is a popular surface modification technique using to repair or remanufacture worn parts operating in high and low temperature environments such as turbine blades, aerospace components, nuclear reactors, automobile engine units, sheet metal forming molds in automotive industry etc. [2,3]. It is suitable for repairing fatigue cracks, corroded, damaged, and worn components. However, this process has some disadvantages such as crack and porosity.

Manjanah et al. [4] studied laser metal cladding with 316L powder material on stainless steel for single-track. They investigated the effects of laser power, scanning speed and powder flow rate on cladding geometry and microstructural details. They observed that the cladding height and width decreased with increasing scanning speed and decreasing laser power. Also, they observed columnar and equiaxed dendritic grains in the direction

of solidification. Pan et al. [5] implemented 18Cr-0.2C Fe- powder on AISI420 stainless steel substrate using laser cladding method. Microstructure, phase transformations, mechanical properties, thermal cycle, corrosion properties were investigated. They observed the lath martensite formed in the microstructure at the top of cladding layer, a portion of the base metal melted during the cladding process and lots of carbides collected in this region causing the existence of a Cr depleted zone. Ferreira et al. [6] investigated multilayer deposited of martensitic stainless steel (Metco 42C) powder on 42CrMo4 structural steel. Laser power, scanning speed and feed rate were tested with preheating and without preheating. The effect of the parameters on the microstructure and microhardness and cladding geometry (height, width, and depth) were analyzed. They found that the metallurgical bonding required higher than 1 kW laser power. The increase in laser power and feed rate enhanced the probability of cracking. But, preheating reduced the crack problems. They stated that the determination of optimal conditions were essential for cladding quality.

In the next years, laser cladding technology is expected to become more extensive in a variety of sectors, including mold repair. But, porosity problems in this method need to be minimized. There are limited studies on multi-layer laser cladding in the literature, mostly researches for a single layer. The purpose of this study is to investigate the effect of process parameters (laser power and scanning speed) on microhardness and porosity in the laser cladding process of martensitic stainless steel powder (Metco 42C) on ductile cast iron (FGS600-3A) used in automotive molds. The porosity rate was calculated by the digital image processing method.

2.   EXPERIMENTAL DETAILS

Metco 42C powder, which corresponds to AISI 431 martensitic stainless steel, was deposited on FGS600-3A ductile cast iron used in sheet metal forming molds by the laser cladding process. **Table 1** shows the chemical compositions of FGS600-3A ductile cast iron and Metco 42C powder used in this study.

Table 1 Chemical composition (wt.%) of Metco 42C powder and FGS600-3A ductile cast iron

Material	C	Si	Mn	P	S	Sn	Cu	Mg	Cr	Ni
FGS600-3A	3.06	2.06	0.52	0.044	0.009	<0.01	0.68	0.049	--	--
Metco 42C	0,18	--	--	--	--	--	--	--	17	2

In the laser cladding process, 6-axis filling welding unit KUKA KR 90 R3100 Extra and the KUKA KL 1500-3T linear table were used in cartesian coordinates (**Figure 1**). LASERLINE-LDF 4000-100 laser has 4000 W of a maximum laser power. The laser beam diameter was 3 mm, and the laser wavelength was 900-1070 nm. Laser beam quality was 30 mm-rad, the minimum focus was 450 µm on 150 mm distance. The software used was Toplas 3D V3. ERLAS Gmbh laser nozzle and DELTATHERM LTK 1-4 Laser Nozzle Cooling Device were used. Fiber cable length was 30 m, optical fiber was 600 µm (NA 0.2), and laser torch workpiece distance was 12 mm.

Figure 1 The laser cladding unit

Laser cladding was implemented under Argon shielding gas which has a flow rate of 5 l/min. Oerlikon Twin-120A Powder Feed has a 13.6 g/min powder flow rate, 3 rpm powder feeder rotation speed. The other technical properties, cooling water flow rate was 1.8 l/min, and cooling water pressure was 0.22-0.3 MPa.

In this study, three test groups were formed (**Table 2 and Figure 2**). Our expertise in commercial applications was beneficial to determine the parameter values used in this study. The energy input was calculated based on laser power and scanning speed (Equation1) [7] :

$$EnergyInput = \frac{LaserPower}{ScanningSpeed} \tag{1}$$
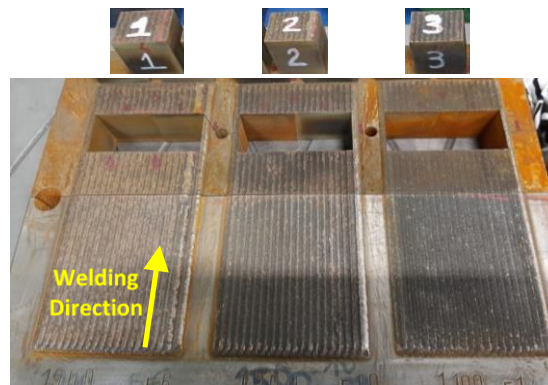
Figure 2 Test specimens produced with different process parameters

Table 2 The laser cladding parameters used in this study

Experiment No	Laser Power (kW)	Scanning Speed (mm/s)	Energy Input (J/mm)
1	1.9	6	316.67
2	1.5	10	150
3	1.1	14	78.57

Laser cladding was implemented to 150 mm x 60 mm in length and width on FGS600-3A molds which were machined 1 mm thickness using a CNC milling machine before laser cladding to obtain a flat surface as in real applications. The cladding was built in three layers, a single layer was approximately 1 mm thick, and the hatch spacing was kept constant at 1.5 mm. The specimens were cut in a cross-section plane (transverse and longitudinal) using an electrical discharge machining (EDM) machine. For layer characterization, it was ground on 180, 400, 600, 800, 1000, 1200 grit SiC papers, and polished 1 μm and 0.3 μm colloidal alumina with FORCIPOL 2V metallographic grinding and polishing machine.

The NIS Elements-D program in the optical microscope was used to quantitatively examine specimen surfaces using the digital image processing approach. The pore fractions of the specimens were determined. Vickers microhardness measurements from the surface along with the depth at 100 μm intervals were taken using a DUROLINE-M hardness tester with a 10s dwell time and 50 g load for transverse surface.

3. RESULTS AND DISCUSSION

3.1. Porosity Analysis

Energy input had a significant influence on the pore formation and shapes in the cladded layers in this study. The energy input have to be controlled to obtain a low porous cladding, since pore formations affect significantly the mechanical properties. The images of the transverse and longitudinal surfaces of the

specimens numbered "1" were shown in (**Figure 3**). The pores based on gases were become large and their fraction has increased because the molten pool flow dynamics have increased through the highest energy input [8-12]. The larger pores were greater the buoyancy in the molten pool. So, it can be seen that the larger pores spread to the upper layers with the increase in energy input (**Figures 3-5**). However, it is understood that, although the cooling rate in the specimen with the highest energy input was the lowest, this cooling rate was not sufficient to get rid of the gases floating in the cladding layer. The images of the cross-sections of the specimen "2" were shown in (**Figure 4**). The pore formation was less than "Specimen 1" due to the medium energy input (lower laser power and higher scanning speed). The images of the cross-sections of the specimen "3" can be also seen in (**Figure 5**). This specimen had the lowest porosity. But, the microcrack formations have appeared in this specimen due to the higher cooling rate (**Figure 5b**). In this study, the pore fractions of the specimens can be seen in **Table 3** and (**Figure 6**). An increase in energy input increases the pore fraction.
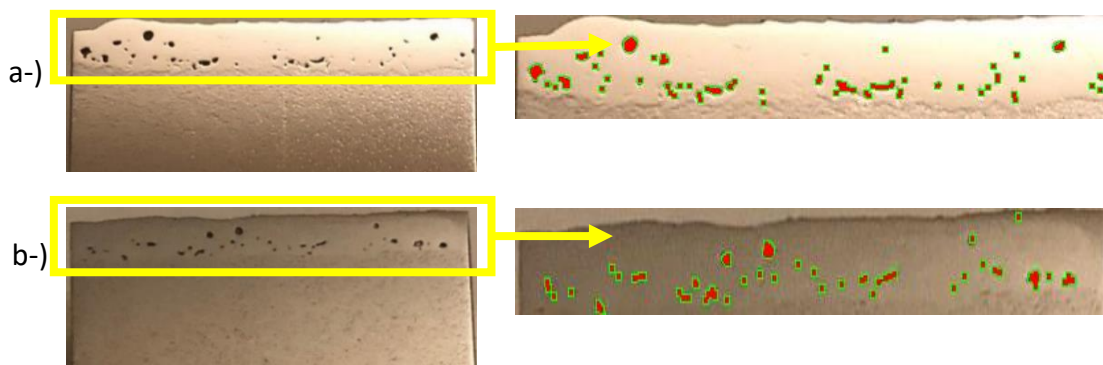
Figure 3 Cross section pore analysis of "Specimen 1" a-) transverse and b-) longitudinal
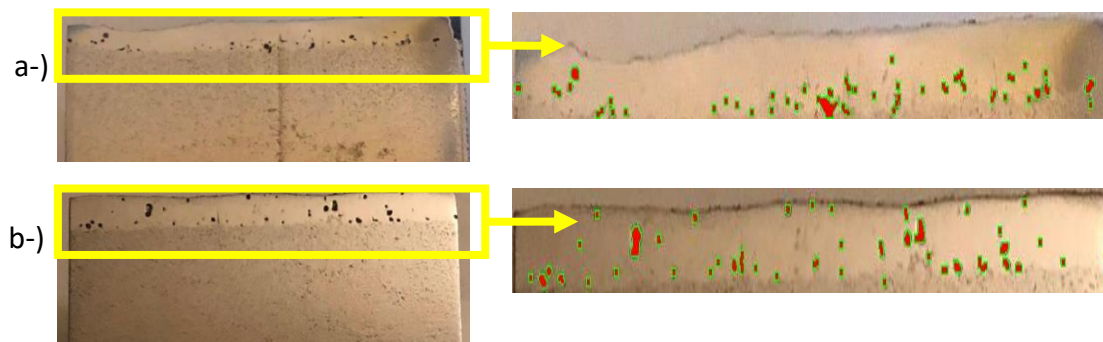
Figure 4 Cross section pore analysis of "Specimen 2" a-) transverse and b-) longitudinal
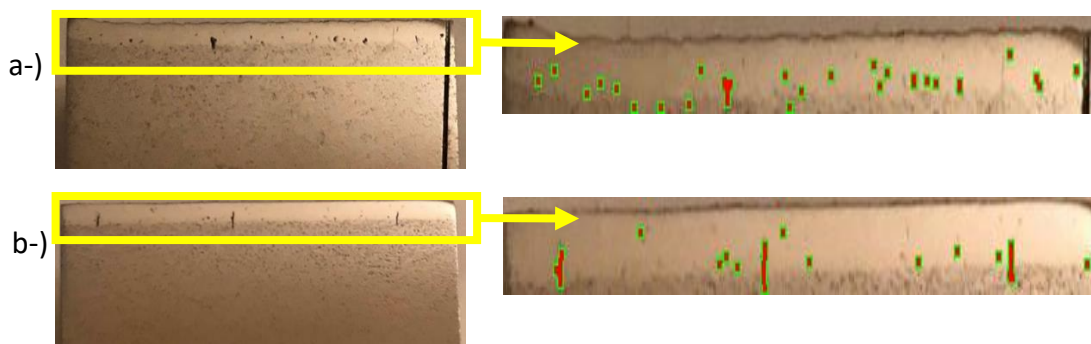
Figure 5 Cross section pore analysis of "Specimen 3" a-) transverse and b-) longitudinal

Table 3 Pore fractions of the specimens

Experiment No	Cross-Section	Energy Input (J/mm)	Pore Area (mm^2)	Cladding Area (mm^2)	Pore Fraction (%)
1	Transverse	316.67	8.55	153.88	5.56
	Longitudinal		3.98	76.56	5.20
2	Transverse	150	3.89	85.73	4.54
	Longitudinal		2.72	53.57	5.08
3	Transverse	78.57	3.92	86.3	4.54
	Longitudinal		1.85	54.29	3.41
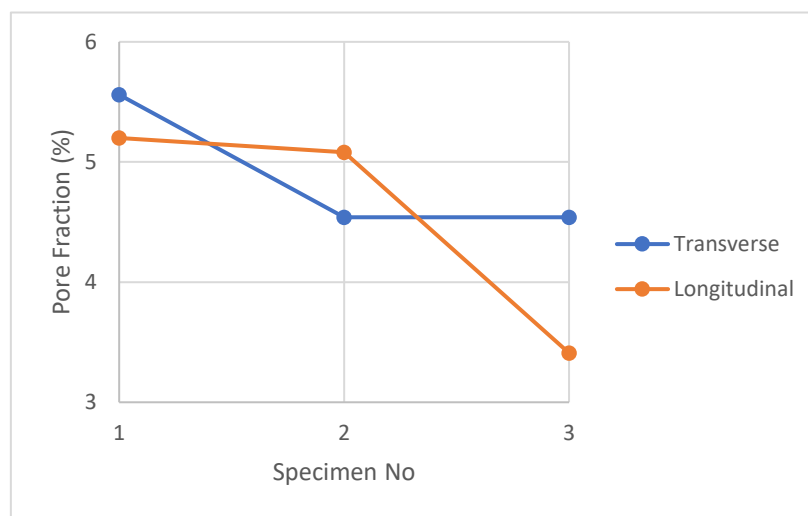
Figure 6 Graphical illustration of pore fractions of specimens

3.2. Microhardness

The microhardness values measured on the cross-sectional surfaces of the specimens are given in **Figure 7**. Cladding layer thickness can be clearly seen with hardness measurements carried out along the depth. The cladding thickness was related to the scanning speed. Since the scanning speed was very low (6mm/s) in the specimen with the highest heat input, the powder efficiency was high and the cladding layer height was higher than the others. The lowest cladding thickness was observed in the specimen produced with a scanning speed of 14 mm/s. In specimen "1" having the highest heat input (1.9 kW, 6 mm/s), hardness values were above 600 $HV_{0.05}$ in the top layer close to the surface having no subsequent thermal cycle. That is, the final cladding layer had not undergone any additional heat treatment cycle. Due to the rapid cooling of powder material after laser cladding, high hardness values were obtained through the occurrence of hard martensitic phases in the microstructure. On the other hand, while the hardness values in the second layer decreased to around 450 $HV_{0.05}$, the hardness value approached around 400 $HV_{0.05}$ in the first layer. The first and second layers were exposed to thermal cycle twice and once during laser cladding deposition, respectively. It was caused the martensite phase to temper, resulting in a reduction in hardness. In specimen "2" having medium heat input (1.5 kW, 10 mm/s), the hardness was approximately 600 $HV_{0.05}$ in the near-surface areas. The hardness values in the second layer decreased to 450-500 $HV_{0.05}$, while the hardness values in the first layer were slightly above 400 $HV_{0.05}$. In specimen "3" having the lowest heat input (1.1 kW, 14 mm/s), the hardness values in the third, second and first layer were 600 $HV_{0.05}$, over 500 $HV_{0.05}$ and 400-450 $HV_{0.05}$, respectively. Since the martensite in the initial two layers was less tempered in this specimen due to lower heat input, the hardness losses as a result of thermal cycling were relatively less than the other specimens.
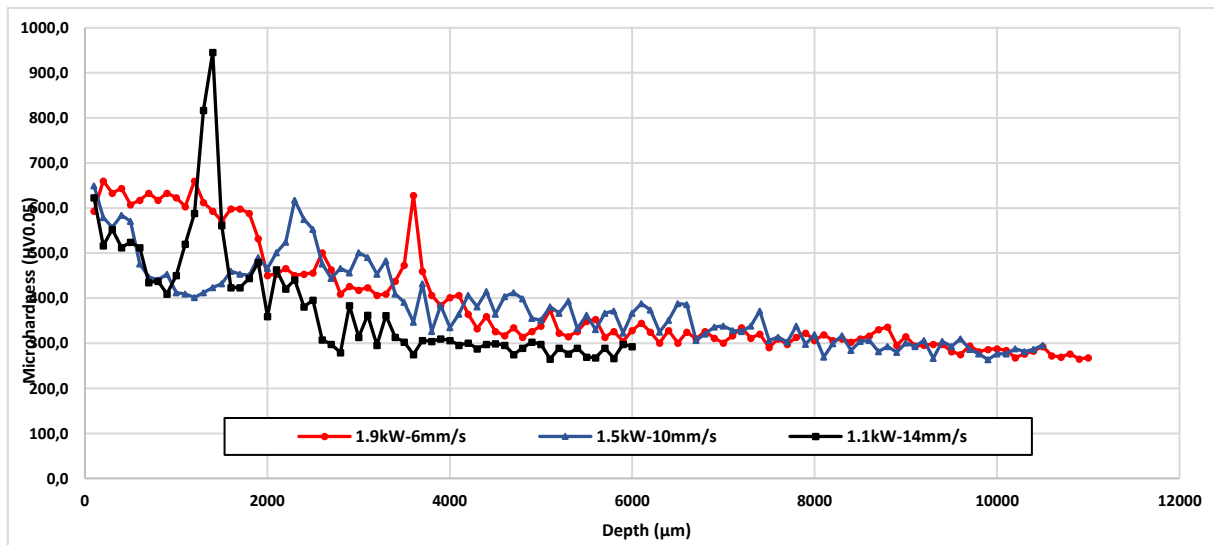
Figure 7 Microhardness measurements of the specimens along the depth

The remarkable increase in hardness from the surface through the depth has occurred at the transition zone that was identified as the fusion zone between the first cladding layer and the base metal. By way of the carbon transfer from the base metal to the cladding zone, the carbon ratio has increased significantly in transition zone. So, the hardness of the martensite phase having higher tetragonality was high in this zone that has a high carbon content. This increase in hardness was very noticeable in the lowest heat input: the microhardness was around 950 $HV_{0.05}$. In other specimens which have higher heat input, the hardness values were roughly 620 $HV_{0.05}$. This can be associated with more tempering of martensite and more carbon transfer from base metal to this zone at higher heat input. So, more carbon led to soft rest-austenite phase. It seems that carbon transfer was not at a level to form rest-austenite in the specimen having the lowest heat input. So, the microstructure in this specimen was completely transformed into the martensitic structure and increased the hardness significantly.

The first layer was the most critical region for crack formation due to embrittlement. The microcracks were observed in the specimen having the lowest heat input with high hardness. Crack risk can be prevented by decreasing the hardness via increasing the heat input and preheating, using different process parameters.

4.   CONCLUSION

In this study, the porosity and microhardness in martensitic stainless steel cladded layer on the FGS600-3A ductile cast iron were investigated in terms of different energy inputs. The conclusions have been drawn as follows:

- Energy input has a significant effect on pore size and fraction. An increase in energy input increases the pore size and fraction. But, the lower energy input increases the risk of microcrack formation in the cladding layer.
- The powder deposition efficiency decreases with increasing scanning speed. So, cladding layer thickness decreases with the increase of scanning speed.
- The upper cladding layer has higher hardness values due to the martensitic structure. Since the first and second layers were exposed to the thermal cycles during cladding process, these layers have lower hardness.
- The transition zone between the first layer and the base metal has a remarkable increase in the hardness. This increase in hardness is very noticeable at lowest energy input. This increase decreases with the increase of energy input.

ACKNOWLEDGEMENTS

REFERENCES

[1] LIAN, G., XIAO, S., ZHANG, Y., JIANG, J., ZHAN, Y. Multi-objective optimization of coating properties and cladding efficiency in 316L/WC composite laser cladding based on grey relational analysis. *International Journal of Advanced Manufacturing Technology*. 2021, vol. 112, pp. 1449–1459. Available from: https://doi.org/10.1007/s00170-020-06486-1.

[2] THAWARI, N., GULLIPALLI, C., KATIYAR, J., GUPTA, T. V. K. Effect of Multi-Layer Laser Cladding of Stellite 6 and Inconel 718 Materials on Clad Geometry, Microstructure Evolution and Mechanical Properties. *Materials Today Communications*. 2021, vol 28, pp. 102604. Available from: https://doi.org/10.1016/j.mtcomm.2021.102604.

[3] GROHOL, C. M., SHIN, Y. C., FRANK, A. Laser cladding of aluminum alloy 6061 via off-axis powder injection. *Surface and Coatings Technology*. 2021, vol. 415, pp. 127099. Available from: https://doi.org/10.1016/j.surfcoat.2021.127099.

[4] MANJAIAH, M., HASCOËT, J. Y., RAUCH, M. Effect of process parameters on track geometry, microstructural evolution on 316L stainless steel multi-layer clads. *Materials Science and Engineering B: Solid-State Materials for Advanced Technology*. 2020, vol. 259, pp. 114583. Available from: https://doi.org/10.1016/j.mseb.2020.114583.

[5] PAN, C., LI, X., ZHANG, R., LU, C., YANG, C., YAO, D. Research on microstructural and property evolution in laser cladded HAZ. *Surface Engineering*. 2021, vol 37, pp. 1-9. Available from: https://doi.org/10.1080/02670844.2021.1929737.

[6] FERREIRA, A. A., DARABI, R., SOUSA, J. P., CRUZ, J. M., REIS, A. R., VIEIRA M. F. Optimization of direct laser deposition of a martensitic steel powder (Metco 42c) on 42crmo4 steel. *Metals*. 2021, vol. 11 , pp. 1–18. Available from: https://doi.org/10.3390/met11040672.

[7] ZHAO, Y., ZHAN, X., ZHOU, X., LIU, T., KANG, Y. Effect of heat input on macro morphology and porosity of laser-MIG hybrid welded joint for 5A06 aluminum alloy. *International Journal of Advanced Manufacturing Technology*. 2021, vol. 115, pp. 4035-4045. Available from: https://doi.org/10.1007/s00170-021-07378-8.

[8] RAHMAN, K. M., AMIN, M. R., MIAN, A. A numerical study of diffusion of nanoparticles in a viscous medium during solidification. *Journal of Thermal Science and Engineering Applications.* 2019, vol. 11, pp. 1–10. Available from: https://doi.org/10.1115/1.4041349.

[9] BRENNAN, M., KEIST, J. S., PALMER, T. A. Defects in Metal Additive Manufacturing Processes. *Additive Manufacturing Processes*. 2020, vol. 30, pp. 277–286. Available from: https://doi.org/10.31399/asm.hb.v24.a0006557.

[10] CULLOM, T., LOUGH, C., ALTESE, N., BRISTOW, D., LANDERS, R., BROWN, B., HARTWIG, T., BARNARD, A., BLOUGH, J., JOHNSON, K., KINZEL, E. Frequency domain measurements of melt pool recoil force using modal analysis. 2021, vol. 11, p. 10959. Available from: https://doi.org/10.1038/s41598-021-90423-z.

[11] WIRTH, F., ARPAGAUS, S., WEGENER, K. Analysis of melt pool dynamics in laser cladding and direct metal deposition by automated high-speed camera image evaluation. *Additive Manufacturing*. 2018, vol. 21, pp. 369–382. Available from: https://doi.org/10.1016/j.addma.2018.03.025.

[12] BAYAT, M., NADIMPALLI, V. K., BIONDANI, F. G., JAFARZADEH, S., THORBORG, J., TIEDJE, N. S., BISSACCO, G., PEDERSEN, D. B., HATTEL, J. H. On the role of the powder stream on the heat and fluid flow conditions during Directed Energy Deposition of maraging steel-Multiphysics modeling and experimental validation. *Additive Manufacturing*. 2021, vol. 43, 102021. Available from: https://doi.org/10.1016/j.addma.2021.102021.